Chemistry–A European Journal
Research Article
doi.org/10.1002/chem.202203469
Chemistry Europe
European Chemical Societies Publishing
www.chemeurj.org

Supramolecular Aggregation Control in Polyoxometalates Covalently Functionalized with Oligoaromatic Groups

Sebastian Knoll,[a] Matthias Hänle,[a] Alexander K. Mengele,[a] Dieter Sorsche,[a] Sven Rau,[a] and Carsten Streb*[a, b]

Abstract: CLICK-chemistry has become a universal route to covalently link organic molecules functionalized with azides and alkynes, respectively. Here, we report how CLICK-chemistry can be used to attach oligoaromatic organic moieties to Dawson-type polyoxometalates. In step one, the lacunary Dawson anion $[\alpha_2\text{-}P_2W_{17}O_{61}]^{6-}$ is functionalized with phosphonate anchors featuring peripheral azide groups. In step two, this organic-inorganic hybrid undergoes micro-wave-assisted CLICK coupling. We demonstrate the versatility of this route to access a series of Dawson anions covalently functionalized with oligoaromatic groups. The supramolecular chemistry and aggregation of these systems in solution is explored, and we report distinct changes in charge-transfer behavior depending on the size of the oligoaromatic π-system.

Introduction

Supramolecular organic-inorganic hybrid systems hold great promise as the next-generation of functional materials.[1,2] In molecular metal oxide (polyoxometalate, POM) chemistry,[3,4] the last decade has seen immense progress in the covalent organo-functionalization of POMs,[5–8] leading to their use in areas ranging from supramolecular chemistry[9–11] and energy conversion/storage[12–14] to electronic nanomaterials[15,16] and covalent POM-bioconjugates.[17,18] POMs are ideal molecular platforms for (bio-)organo-functionalization, as they introduce redox-,[19] photo-,[20] catalytic[21] and magnetic activity.[22] To-date, the covalent functionalization and post-functionalization of POMs is still challenging and requires the combination of specific POM structure types with suitable organic anchoring groups.[5–8]

One promising approach to overcome this bottleneck is the introduction of organic azide functions covalently attached to the POM,[23–25] so that subsequent CLICK chemistry[26] (i.e., copper catalyzed alkyne-azide cycloaddition) enables versatile post-functionalization. To access "CLICKable" POMs, different cluster architectures have been covalently functionalized with organic azides, including the Anderson anion[23,27] as well as the Dawson anion.[28,29] In one recent example, Dietzek-Ivanšić, Rau and Streb showed how ruthenium-based photosensitizers can be covalently linked to Dawson anions via phosphonate anchors.[30] The group reported that careful choice of synthetic conditions was required, together with the use of protecting group strategy to enable clean access to the resulting photo-sensitizer-POM dyad. The resulting molecular system was capable of storing electrons and releasing them to facilitate hydrogen evolution on demand even in the dark. However, this study also highlighted the challenges related to designing complex organic-inorganic architectures with respect to synthetic feasibility as well as stability.[5,6]

To address these challenges, we decided to explore whether supramolecular aggregation between photosensitizer and POM can be used as an alternative design approach, allowing more flexibility in terms of component selection and modular design. Thus, we were aiming at accessing POMs covalently functionalized with oligoaromatic systems of different size to explore their supramolecular solution chemistry, as a foundation for supramolecular charge-transfer and charge-aggregation systems. We propose that the resulting systems could act as electron storage sites or electron relays, and in addition the pyrene system is capable of supramolecular (π-π stacking) interactions with complementary molecules such as photo-sensitizers or electron donors in solution.

To-date, POMs featuring oligoaromatic groups have mainly been developed as a means of anchoring the POM to nano-structured carbon substrates such as single-walled carbon nanotubes or graphene for electrochemical applications.[31,32] In addition, covalent attachment of porphyrin-based aromatic systems to POMs have been employed for photoinduced energy and electron transfer between porphyrin and POM.[33]

Here, we report a new synthetic route to bifunctional organic azides featuring a phosphonic acid as POM anchoring

[a] S. Knoll, M. Hänle, Dr. A. K. Mengele, Dr. D. Sorsche, Prof. Dr. S. Rau, Prof. Dr. C. Streb
Institute of Inorganic Chemistry I
Ulm University
Albert-Einstein-Allee 11, 89081 Ulm (Germany)
E-mail: Carsten.streb@uni-mainz.de
[b] Prof. Dr. C. Streb
Department of Chemistry
Johannes Gutenberg University Mainz
Duesbergweg 10–14, 55128 Mainz (Germany)

Supporting information for this article is available on the WWW under https://doi.org/10.1002/chem.202203469

site. We demonstrate that this system can undergo subsequent CLICK-chemistry to enables attachment of oligoaromatic side-groups. Solution studies illustrate the supramolecular interactions of the species with ruthenium complex photosensitizers and highlight how the size of the oligoaromatics controls the photophysical properties of the resulting systems. This work therefore lays the foundation for utilizing organo-functionalized POMs as reactive components in solution-based supramolecular energy conversion and storage systems.[34–36]

Results and Discussion

First, we targeted the phosphonate tether **P2** which combines a CLICKable azide moiety with an established POM phosphonate anchoring group. **P2** was initially synthesized based on a reported route (Figure 1, Route A, top).[25]

An alternative, mild synthetic route was developed via the protected phosphonate ester **P2a** (Figure 1, Route B, bottom). Route A proceeds by deprotection of the phosphonate ester with hydrochloric acid to give the phosphonic acid **P1**, followed by conversion of the amine into an azide via diazotation and subsequent nucleophilic aromatic substitution. Route B initially introduces the azide by substitution of the amine (**P2a**), followed by conversion of the phosphonate ester into an activated silyl species and subsequent hydrolysis (see Supporting Information for synthetic details).

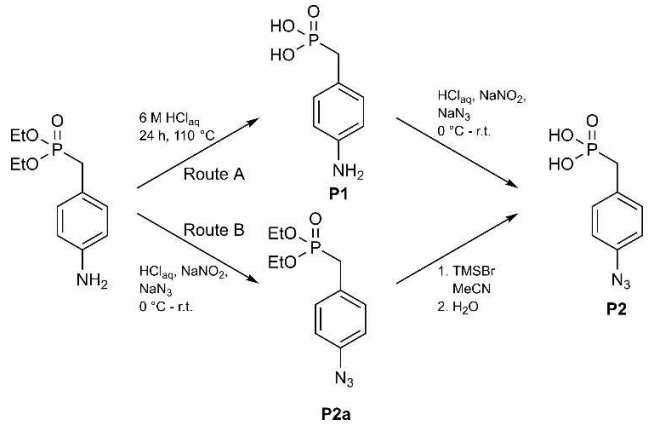

Figure 1. Synthesis of the bifunctional phosphonic acid-azide tether via the literature-known Route A[25] and via the new, room temperature Route B.

Both routes give near quantitative yields of **P2**. However, the new Route B allows preparation of **P2** under milder conditions (Route A: maximum temperature: 110 °C; Route B: maximum temperature: room temperature) so that in future, sensitive functional groups can be introduced via Route B. For synthetic and analytical details see Supporting Information.

The organic azide was covalently anchored to the lacunary α_2-Dawson cluster (nBu$_4$N)$_9$K[α_2-P$_2$W$_{17}$O$_{61}$] (**C1**)[15] by reacting both components (molar ratio 3.3 : 1; azide : cluster) in heated (T = 110 °C) N,N-dimethyl acetamide solution containing 0.4 M HCl$_{aq}$ for 24 h (Figure 2). After workup (details see Supporting Information), the product, (nBu$_4$N)$_6$[α_2-P$_2$W$_{17}$O$_{61}$(POCH$_2$C$_6$H$_4$N$_3$)$_2$] (**CP1**) was obtained as a yellow solid in 80% yield based on (nBu$_4$N)$_9$K[α_2-P$_2$W$_{17}$O$_{61}$] (**C1**). **CP1** was fully characterized by ^{1}H- and ^{31}P NMR spectroscopy (Figures S24 and S25, Supporting Information), and ATR-FTIR spectroscopy (Figure 3 and Figure S26 in Supporting Information) to verify the presence of the azide group.

Post-functionalization of **CP1** was achieved by microwave-assisted copper(I)-catalyzed alkyne-azide cycloaddition (CLICK-chemistry). To this end, **CP1** was reacted in a microwave setup with the three model oligoaromatic alkynes, i.e., phenyl acetylene, 1-ethinyl naphthalene and 1-ethinyl pyrene in cyclohexanone in the presence of the air-stable copper(I) catalyst **Cu1** (details see Supporting Information).[37,38] After workup, this resulted in the pure compounds **CP2**, **CP3** and **CP4**, which were characterized by ^{1}H- and ^{31}P NMR spectroscopy (Figures S30–S35, Supporting Information), as well as ATR-FTIR (Figure S36, Supporting Information).

The successful CLICK-reaction is indicated by characteristic singlet signals in the ^{1}H NMR spectra (between 9.24 and 9.45 ppm, see Figures S30, S32 and S34 in Supporting Information), corresponding to the 1,4-disubstituted triazole. Conversion of the azide is further corroborated by loss of the characteristic azide absorption in the IR spectrum at 2111 cm^{-1} with simultaneous emergence of a triazole absorption feature at 1519 cm^{-1} (Figure 3).[39] Retention of the cluster structure is supported by analysis of the IR fingerprint region, where characteristic W–O–W stretching vibrations between 730 and 820 cm^{-1}, W=O stretches at 955 and 906 cm^{-1}, and P–O stretches at 1085 and 1056 cm^{-1} are observed (see Figure S36,

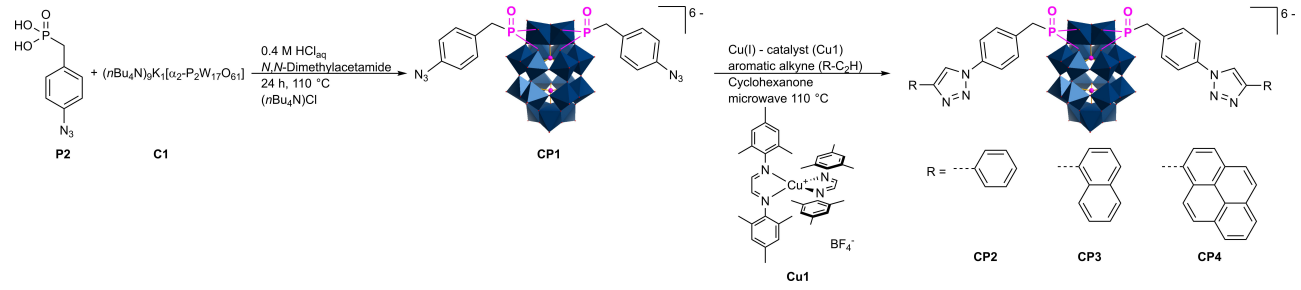

Figure 2. Synthesis of the azide-functionalized α_2-Dawson type POM (**CP1**) and the "clicked" hybrid polyoxometalates (**CP2**, **CP3**, **CP4**), nBu$_4$N$^+$ counterions are omitted for clarity.

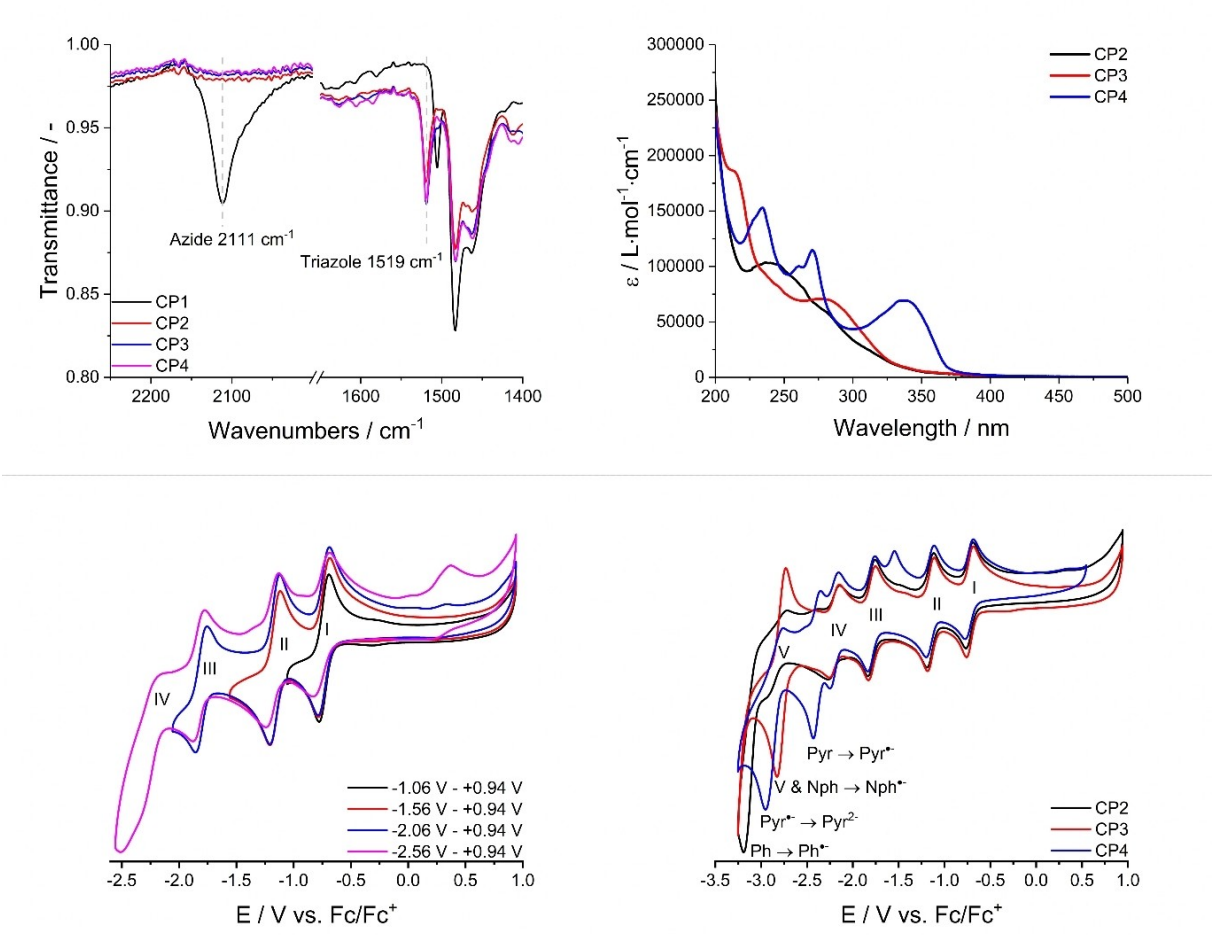

Figure 3. Top left: ATR-FTIR spectra of **CP1** before and **CP2**, **CP3** and **CP4** after the CLICK-reaction; top right: UV-Vis spectra of **CP2**, **CP3** and **CP4** in acetonitrile; bottom left: cyclic voltammetry of **CP1**; bottom right: cyclic voltammetry of **CP2**, **CP3**, **CP4**. Conditions: [POM] = 1.0 mM; solvent: de-aerated, water-free DMF containing 0.1 M $(nBu_4N)PF_6$ as supporting electrolyte.

Supporting Information). The ^{31}P NMR spectra show three singlets, one corresponding to the phosphonate anchor ($\delta =$ 22.4 ppm), the other two corresponding to the internal phosphate templates ($\delta = -11.3$ and $\delta = -12.9$ ppm, see Figures S31, S33 and S35, Supporting Information,).

The electronic absorption spectra of **CP2**, **CP3** and **CP4** (Figure 3) show characteristic absorption bands in the near-UV region, which are assigned to $O \rightarrow W^{VI}$) ligand-to-metal charge-transfer (LMCT) bands of the POM. Additional spectral features in the UV region are assigned to $\pi \rightarrow \pi^*$ transitions of the aromatic moieties; with increasing size of the aromatic systems, these absorptions shift into the visible range.[40,41] The redox-properties of the organo-functionalized α_2-Dawson clusters **CP1**, **CP2**, **CP3** and **CP4** were investigated by cyclic voltammetry. **CP1** shows two reversible tungsten based ($W^{VI/V}$) redox waves at $E_{1/2} = -0.72$ and -1.15 V vs. Fc/Fc^+, as well as one quasi-reversible $W^{VI/V}$ process at $E_{1/2} = -1.79$ V vs. Fc/Fc^+. When the potential window is extended to -2.00 V and further to -2.50 V. A, a fourth barely observable tungsten-based process (literature known)[29,42] appears, which is partially covered by an irreversible azide-based process at E ca. -2.50 V vs. Fc/Fc^+. Based on the literature, this azide-process can be assigned to the formation of an azide radical anion and the subsequent decay into the respective nitrene radical anion combined with the eventual reaction of the generated nitrene with the solvent (DMF).[43] Formation of these degradation products, i.e., R-$C_6H_4NH^-$ or R-$C_6H_4(N^-)C(O)N(CH_3)_2$ is accompanied by the appearance of new irreversible redox events in the oxidative region ($E = 0.37$ V vs. Fc/Fc^+).[44] In contrast to the non-CLICK-functionalized **CP1**, the species **CP2, CP3 and CP4** show four reversible tungsten-based redox events (Figure 3, **I–IV**), which is in line with related species reported previously.[29,42] A fifth cluster-based reduction (**V**), is expected from literature, but was not unambiguously observed due to overlap with ligand-based redox processes.[29,42] For **CP2**, one irreversible process at $E_{red} = -3.19$ V vs. Fc/Fc^+ is observed, assigned to reduction of the phenyl substituent to a phenyl radical anion. In contrast, **CP3** shows a reversible one-electron reduction of the naphthyl moieties at $E_{1/2} = -2.78$ V vs. Fc/Fc^+, which is in good agreement with the literature.[45] **CP4** shows two reduction processes, assigned to the reduction of pyrenyl to a pyrenyl radical anion (quasi-reversible, $E_{1/2} = -2.40$ V vs. Fc/Fc^+) and reduction of the

pyrenyl radical anion to the two-electron-reduced pyrenyl dianion (irreversible, $E_{red} = -2.85$ V vs. Fc/Fc^{+}), both processes are in good agreement with the literature.[45,46] The systematic anodic shift of the reduction potentials assigned to the aromatic systems of **CP2, CP3** and **CP4** reflects the decreasing LUMO energies due to extension of the aromatic structure from benzene to naphthalene to pyrene. Interestingly, re-oxidation of the pyrene radical anion was found to split up into two separate processes. One explanation could be the interactions between a reduced and a non-reduced pyrene to form dimeric aggregates.

Emission quenching studies

The presence of aromatic moieties offers an opportunity to employ supramolecular π-stacking interactions for the assembly of supramolecular aggregates. To test this concept, we probed the light-induced interactions between the POMs **CP2**, **CP3** and **CP4**, and two ruthenium polypyridyl model photosensitizers as molecular probes using emission spectroscopy. $[Ru(tbbpy)_2(tpphz)](PF_6)_2$ (ruthenium(II)-bis(4,4′-di-*tert*-butyl-2,2′-bipyridyl)-(μ-tetrapyrido [3,2-a:2′,3′-c:3″,2″-h:2‴,3‴-j] phenazine)-bis-hexafluorophosphate) (**PS1**) was selected as a cationic photosensitizer with a large polyheteroaromatic ligand suitable for electrostatic and π-stacking interactions. $[Ru(tbbpy)_3](PF_6)_2$ (tris(4,4′-di-*tert*-butyl-2,2′-bipyridine)ruthenium(II)-bis-hexafluorophosphate) (**PS2**) was used as a reference photosensitizer which does not feature an extended π-aromatic system, interactions are therefore mainly limited to electrostatics (Figure 4).[47,48]

To assess the emission quenching, **PS1** and **PS2** were titrated with 0–1 equivalents of **CP2**, **CP3** or **CP4** in aerated acetonitrile. For **PS1**, efficient emission quenching is observed for all three clusters, and full quenching is observed at molar ratios of ca. 4:1 (**PS:CP**), suggesting that each cluster is capable of interacting with multiple photosensitizer units simultaneously (Figure 5, top). In contrast, for **PS2**, emission quenching was significantly lower (Figure S37, Supporting Information) and at equimolar concentrations (PS:CP = 1:1), residual emis-

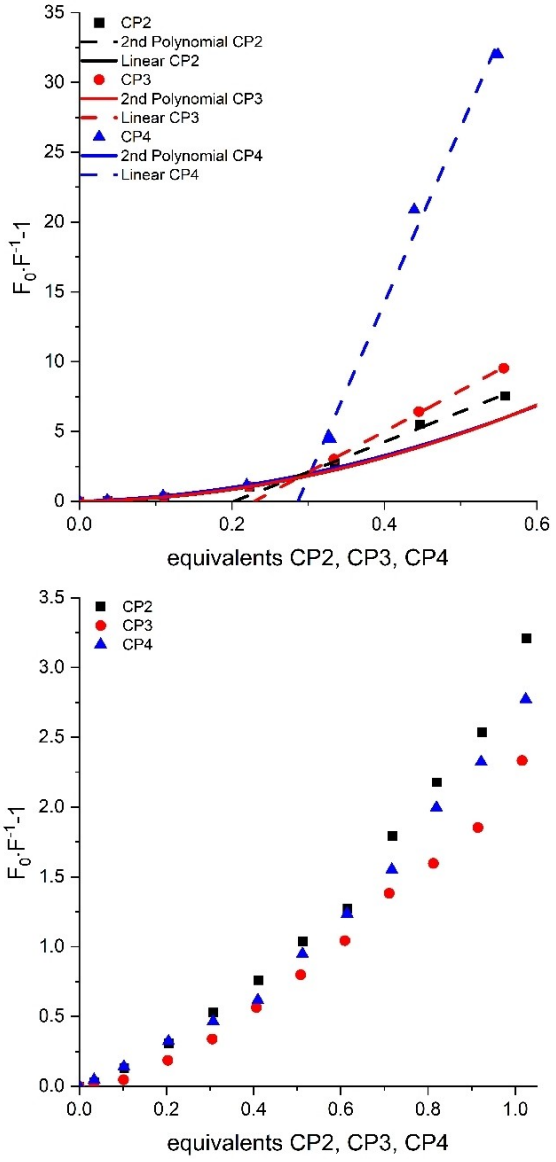

Figure 5. Stern-Volmer plot of $[Ru(tbbpy)_2tpphz](PF_6)_2$ (**PS1**, **top**) and $[Ru(tbbpy)_3](PF_6)_2$ (**PS2**, **bottom**) with **CP2**, **CP3** and **CP4** as quenching molecules in acetonitrile.

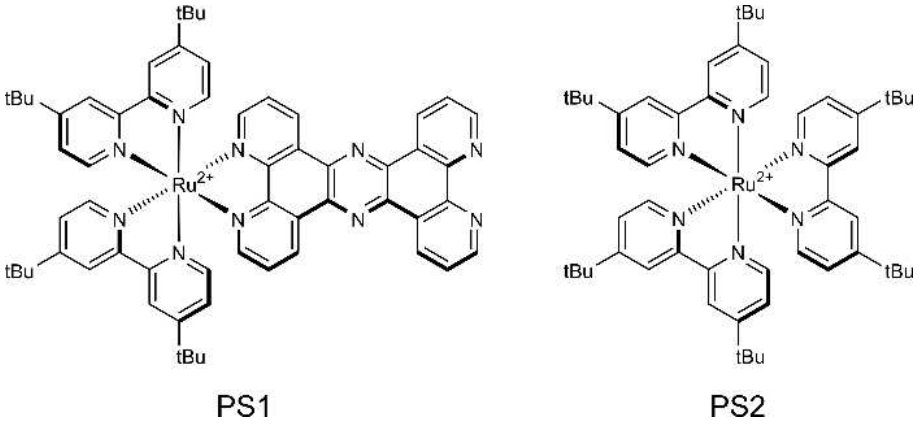

Figure 4. Ruthenium chromophores **PS1** (left) and **PS2** (right).

sion of ~30% of the initial value was still observed (Figure 5, bottom). Furthermore, for **PS2**, the quenching behavior was largely independent of the exact cluster type, **CP2**, **CP3** or **CP4**. This indicates that the solution interactions between photosensitizer and cluster are not affected by the organic aromatic groups but are dominated by electrostatics. **PS2** shows non-linear quenching behavior, indicating both dynamic and static contributions – the latter most likely indicative of the formation of ion pairs through electrostatic interactions.[48,49] In contrast, **PS1** shows a similar but more pronounced effect at low equivalents of **CP**, followed by an almost linear increase at **PS**:**CP** ratios $<4:1$. The slope in this region increases with the size of the aromatic ring systems in **CP2**, **CP3** and **CP4**. In sum, this study demonstrates that controlling the size of the aromatic systems of the functionalized POM anions can be effectively used to control supramolecular solution interactions and thus energy or charge-transfer between PS and POM.

NMR titrations

To further confirm the presence of π-interactions between the oligoaromatic ligands of **CP2**, **CP3** or **CP4**, and **PS1**, NMR titrations were performed using only the ligands **P3**, **P4** and **P5** (Figure 8, see Synthesis and Characterization in Supporting Information) to prevent ion-pair formation of the highly anionic clusters with the cationic **PS1**; thus, it is possible to study the π-stacking interaction without interference by electrostatic aggregation (at high concentrations, the anionic POM and cationic Ru complex form insoluble precipitates). In all NMR studies, the **PS1** concentration was kept constant, while the concentrations of **P3**, **P4** or **P5** were increased. Interactions were analyzed by measuring the relative chemical shift ($\Delta\delta = \delta\text{-}\delta_0$) of the protons H_c and $H_{c'}$ of the tpphz ligand, see Figure 8. While virtually no shifts are observed ($\Delta\delta$ ca. 0.05 ppm at 20 equivalents) for the titration of **PS1** with **P3** and **P4** (phenyl, naphthyl derivates), the titration with **P5** (pyrenyl derivative) leads to a significant shift of up to $\Delta\delta = 0.64$ ppm at 20 equivalents for the proton H_c and $\Delta\delta = 0.53$ ppm at 20 equivalents for proton H_c'. Fitting of the binding isotherms was performed using the bindfit program[50,51] based on the NMR 1:1 model (see Supporting Information for Fit and Residuals). The **P5** derivative fit gave a value of $K_a = 65.08 \pm 0.28\ M^{-1}$, which is in good agreement with a previously published system ($[(tbbpy)_2Ru(tpphz)PdCl_2](PF_6)_2$ + pyrene)[48] where $K_a = 155 \pm 44\ M^{-1}$ was reported. Due to the small NMR shifts for **P3** and **P4** the determination of the association constants is not meaningful and was not performed, leading to the result, that no significant stacking interaction is observed for either **P3** or **P4**. NMR titration data for **P3**, **P4** and **P5** are consistent with the emission data obtained from systems **CP2**, **CP3** and **CP4**. Pyrene functionalization shows strong supramolecular binding to the tpphz ligand which leads to the best emission quenching performance, supporting the hypothesis of efficient π stacking between **PS1** and **CP4**. In contrast, **CP1**, **CP2** and **CP3** feature smaller aromatic systems, leading to interactions with **PS1** which are dominated by electrostatics. In consequence, the emission quenching is less pronounced compared to **CP4** and no binding constants could be determined when using the ligands **P3** and **P4**.

Photochemical reduction

To verify that the observed emission quenching is a result of electron transfer from the photo-excited redox chromophore to the cluster, we performed UV-Vis absorption spectroscopic studies. In particular, we were interested in studying whether charge-accumulation by reduction of the POM is possible under irradiation in the presence of a sacrificial electron donor, i.e., 1,8-diazabicyclo[5.4.0]undec-7-ene (DBU). Initial studies showed that DBU does not quench the emission of **PS1** (see Figure S38, Supporting Information), and therefore does not interfere in possible photochemical reactions of photosensitizer and POM (i.e., the photochemical process will proceed via an oxidative quenching pathway). Also, note that DBU does not reduce the POM clusters employed under irradiation (see Figure S45, Supporting Information).

To study the system, mixtures of the respective POM (**CP2**, **CP3** or **CP4**, 1 equiv.) and the respective photosensitizer (**PS1** or **PS2**, 2.00 equiv.) were irradiated at $\lambda = 470$ nm (LED light source) in acetonitrile in the presence of an excess of DBU (74444 equiv. based on the POM cluster) as electron donor. Corresponding time-lapse absorption spectra for the four systems are shown in Figure 6 and reveal two main processes, i.e., a bathochromic shift of the MLCT absorption of the chromophore, and a broad increase in the area above 470 nm.

A possible mechanism is shown in Figure 7, assuming similar time constants for the photo reductive conditions as they were determined for the pure **PS1**. In step one, the ruthenium photosensitiser **PS1** is excited and a ^{3}MLCT state is generated, which can undergo a fast intra-ligand charge transfer (ILCT) to the phenanthroline unit within 1.2 ps and subsequently an intra ligand charge transfer to the phenazine unit with 240 ps, generating a delocalized radical-anion as a charge separated state (PS*).[52] This can explain the bathochromic shift in the MLCT region as well as a new band appearing between 500 and 600 nm, corresponding to the formed reduced tpphz species. A decrease in intensity and the formation of an isosbestic point (Figure 6D) over time suggests that an additional species is formed during irradiation of **PS1** in the presence of DBU. However, we were note able to isolate or identify this species, therefore the determination of extinction coefficients for these species were not possible.

This decrease in intensity as well as the band shift of the ^{3}MLCT during ligand (tpphz) reduction was also observed in photoreductions containing **CP1**, **CP2** and **CP3** but not **CP4**, suggesting that for **CP4**, this process is not possible.

Step two involves a charge transfer from the photosensitizer to the POM, resulting in a characteristic, POM-based ($W^{VI/V}$) intervalence charge-transfer (IVCT) transition, centred around 840 nm (IVCT1) and 650 nm (IVCT2). An exergonic electron transfer from **PS1** to cluster is proposed by simple comparison of the electrochemical potentials. A reductive potential of −1.39 V[53] vs. Fc/Fc^+ is featured by the phenazine unit. The two

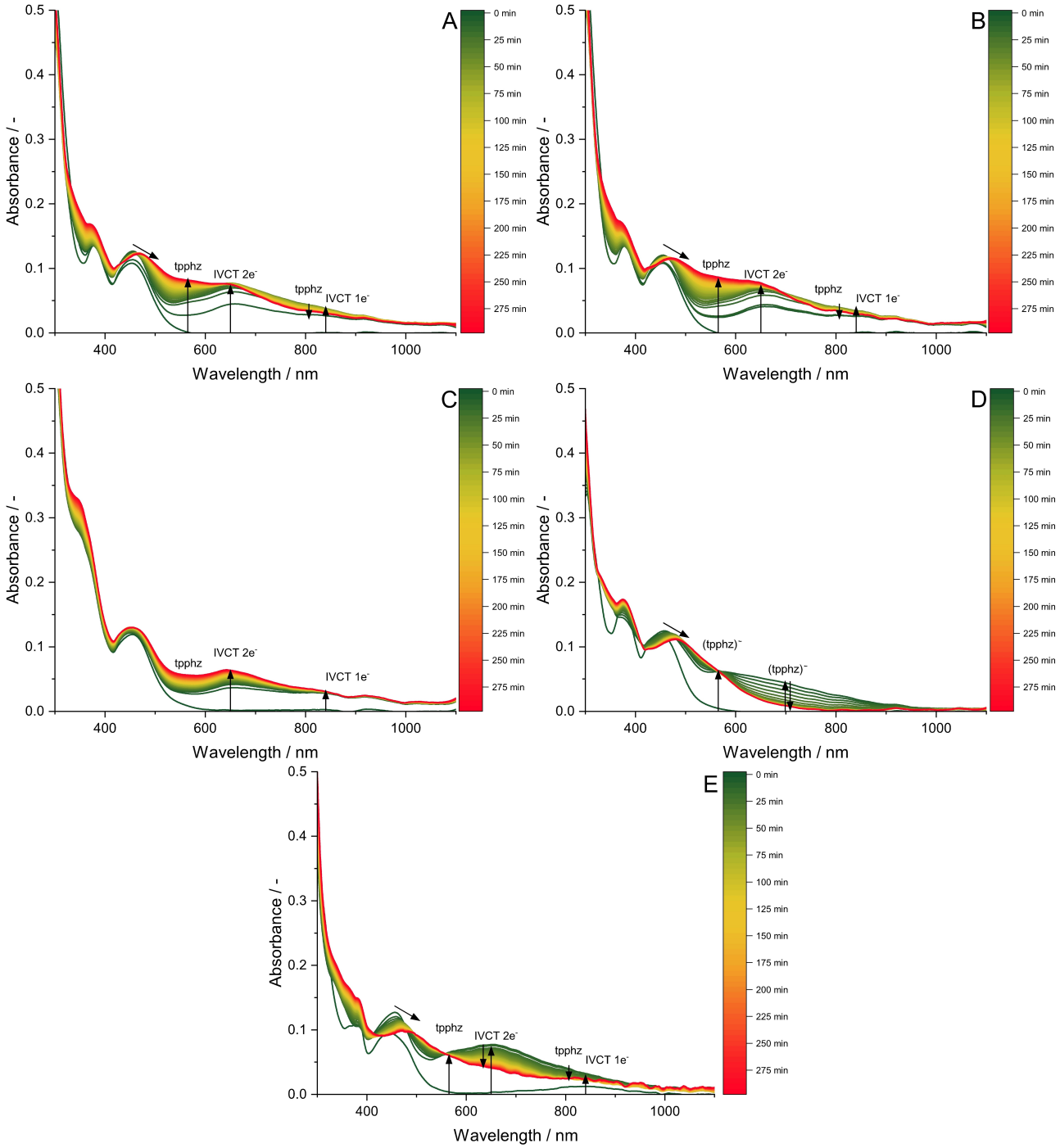

Figure 6. Time lapse UV-Vis spectra during photo electron transfer of clusters. A) **CP2**, B) **CP3** and C) **CP4** with DBU and $[Ru(tbbpy)_2tpphz](PF_6)_2$ (**PS1**), D) $[Ru(tbbpy)_2(tpphz)](PF_6)_2$ with DBU and E) **CP1** with DBU and **PS1** as Reference (experimental details included in Section "Photochemical Reduction", Supporting Information).

relevant reduction potentials of **CP1** to **CP4** are observed at −0.72 and −1.15 V vs. Fc/Fc^+. In both cases the reduced phenazine unit features a low enough potential to transfer electrons to the cluster. As the third cluster reduction event shows a more negative potential (−1.79 V vs. Fc/Fc^+) compared to the phenazine unit, an exergonic electron transfer step, resulting in a third reduction of the POM is not possible.

In step three, the photosensitizer is regenerated by reduction with the sacrificial electron donor DBU. This process is repeated, so that eventually, the two-electron reduced cluster systems are obtained. At low concentrations of reduced clusters, the charge transfer rate between the tpphz-radical anion and the cluster is higher than generation of reduced tpphz. At a certain point, the concentration of reduced cluster

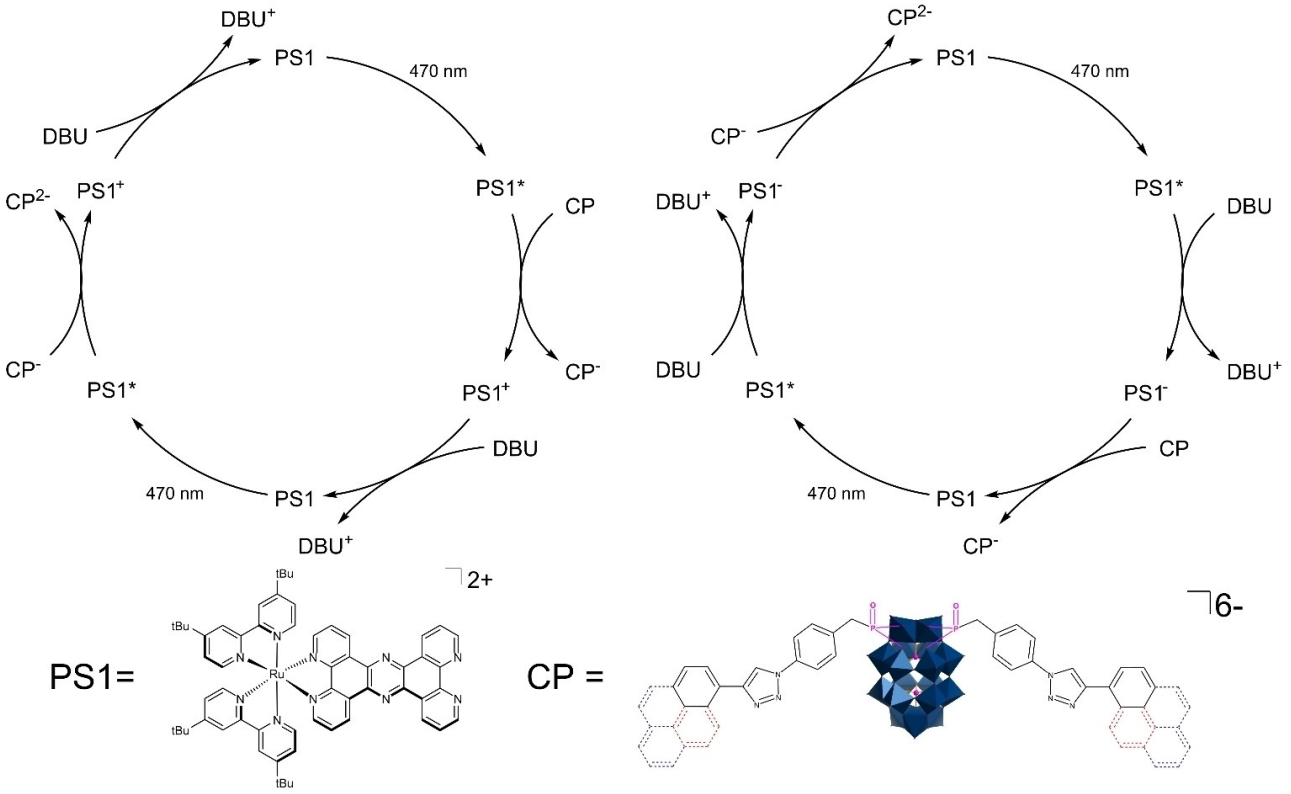

Figure 7. Proposed photoreduction mechanism for organo-phosphonate functionalized Dawson cluster [**CP2** (black), **CP3** (red), **CP4** (blue)] by **PS2** as photosensitizer and DBU as sacrificial electron donor. left: cluster reduction and PS regeneration; right: PS regeneration and cluster reduction (PS1* represents the charge separated state Ru^{III} tpphz^{-}).

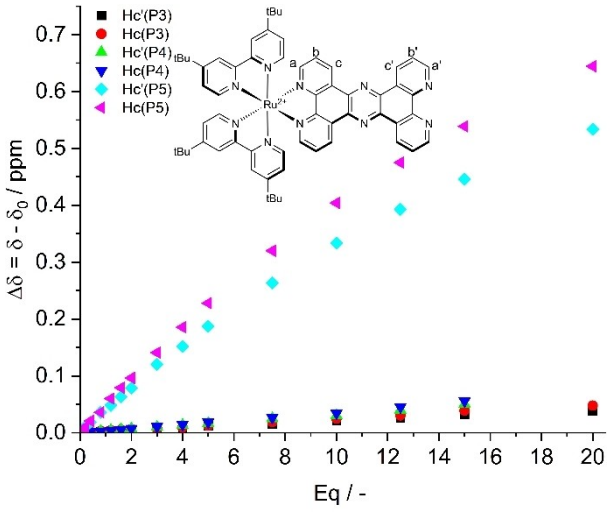

Figure 8. NMR-titration of **PS1** with oligoaromatic ligands **P3**, **P4** and **P5** for protons H_c and H_c'.

increases and the charge transfer rate decreases, leading to a charge accumulation at the PS, as thermodynamically, no further electron transfer to the POM is possible. **CP2** and **CP3** both show two-electron reduction within 60 minutes as shown in Figure 6A and B (indicated by the characteristic signal at 650 nm, IVCT transition of the two-electron reduced species). After 60 minutes, no further increase of the intervalence charge transfer band is detected and only the formation of the reduced phenazine species is observed (compare Figure 6A, B and D). **CP1** shows a significantly faster electron transfer to the cluster, indicated by the IVCT process at 650 nm (Figure 6E). Also, we note the rapid reductive breakdown the tpphz ligand (shown by the bathochromic shift in the MLCT region as well as the appearance of a band between 500 nm and 600 nm). In addition, the fast decrease of the band at 650 nm, could be indicative of a possible breakdown of the whole **CP1** cluster. Comparison of the final reaction states of the **CP1** reduction and the reduction of **PS1** show notable similarities, which indicates that the spectral features are dominated by the signals of the reduced photosensitizer rather than the reduced POM cluster. Interestingly, cluster **CP4** shows a more complex behavior upon irradiation in presence of **PS1** and DBU. Specifically, formation of the two-electron reduced cluster species at 650 nm (two-electron reduced IVCT) appears to continue beyond 60 minutes, as characterized by the continuous increase in IVCT absorption intensity. At the same time, accumulation of the reduced phenazine species is virtually not observed. Figure S43(A–D) shows the time dependent difference spectra, showing more clearly the difference between the three clusters as well as **PS1**. Control experiments regarding photo-reactions of individual components can be found in the Supporting Information (Figures S44 and S45).

Also, a dependence of the efficiency of electron transfer between the cluster **CP1**, **CP2**, **CP3** and **CP4** with complex **PS1** could be observed. This is generally in agreement with results from the emission spectroscopy experiments, showing that, the more extended the size of the aromatic π-system, the more efficient is the quenching of the excited ruthenium complex and thus, the better the electron transfer. This supports the hypothesis of π-stacking effects between the polyheteroaromatic ligand in **PS1** and the pyrene functionalized cluster **CP4**. However, fast photoreduction is also observed for **CP1** to **CP3** where no significant p stacking is observed in the NMR titration experiments, and where emission quenching is rather low compared to **CP4**. This suggests that electrostatic aggregation by itself can be used to trigger photoreduction; however, we note that in these systems (**CP1**–**CP3**), we observe fast photodegradation of the aromatic system and loss of chemical stability, while **CP4** is more stable. It can therefore be proposed that efficient π-stacking of **PS1** and **CP4** improves both the stability of the reduced cluster system as well as the stability of the polyheteroaromatic ligand in **PS1**.

In contrast to **PS1**, experiments involving chromophore **PS2** show bleaching of the MLCT excitation and concomitant formation of a new absorption at 570 nm (Supporting Information, Figure S49), which likely corresponds to a new ruthenium complex rather than cluster reduction (see Supporting Information for more information), as characterized by the respective shape and intensity of the absorption band. $[Ru(bpy)_3]^{2+}$ or $[Ru(tbbpy)_3]^{2+}$ (**PS2**) are known to undergo rapid photodegradation upon population of a metal-centered ^{3}MC state,[54] which leads to loss of a bipyridine ligand and follow-up reactions. The degradation of **PS2** is also supported by the fact that no photoreduction of the POM clusters was observed, which can be correlated to the fact that **PS2** does not feature an extended aromatic system for supramolecular interactions with the POM. Further analyses including hetero-sample-correlation spectroscopy see Supporting Information (2D Hetero-Sample-Correlation Spectra).

Conclusion

In summary, we demonstrate how supramolecular assembly and light-driven electron transfer can be controlled by covalent functionalization of POMs with oligoaromatic moieties. A facile synthesis based on CLICK chemistry was used to access Dawson POMs with oligoaromatic substituents. Systematic study of the effects of size of the aromatic system on the photophysical and electronic properties of the resulting dyads lays the foundation for tuning and optimization of reactivity in this compound class. The study also shows how supramolecular π-stacking interactions lead to a shift in electron transfer dynamics, leading to more efficient charge accumulation. Future studies will be focused on the synthetic development of these systems. Their integration into functional light-harvesting and energy conversion/storage systems can be envisaged based on the fundamental synthetic concepts and mechanistic understanding presented in this study.

Experimental Section

Full analytical, spectroscopic and crystallographic details are given in the Supporting Information.

Deposition Number(s) 2215278 contain(s) the supplementary crystallographic data for this paper. These data are provided free of charge by the joint Cambridge Crystallographic Data Centre and Fachinformationszentrum Karlsruhe Access Structures service.

Acknowledgements

The authors gratefully acknowledge the Deutsche Forschungsgemeinschaft DFG for financial support (projects TRR 234 "CataLight", project no: 364549901; SPP2102, "Light-controlled reactivity of metal complexes", project no: 359737763, 494988281). S.K. gratefully acknowledges a LGFG PhD fellowship by the State of Baden-Württemberg.

The data that support the findings of this study are openly available in the open repository zenodo.org at https://doi.org/10.5281/zenodo.7256944. Open Access funding enabled and organized by Projekt DEAL.

Conflict of Interest

The authors declare no conflict of interest.

Data Availability Statement

The data that support the findings of this study are openly available in zenodo.org at The data that support the findings of this study are openly available in the open repository zenodo.org at https://doi.org/10.5281/zenodo.7256944, reference number 7256944.

Keywords: organic-inorganic hybrid · organofunctionalization · photosensitizer · polyoxometalate · supramolecular

[1] S. Erbas-Cakmak, D. A. Leigh, C. T. McTernan, A. L. Nussbaumer, *Chem. Rev.* **2015**, *115*, 10081–10206.
[2] Q. Zhang, D.-H. Qu, H. Tian, B. L. Feringa, *Matter* **2020**, *3*, 355–370.
[3] M. T. Pope, A. Müller, *Polyoxometalate Chemistry: From Topology via Self-Assembly to Applications*, Kluwer Academic Publishers, Dordrecht; Boston, **2001**.
[4] L. Cronin, A. Müller, *Chem. Soc. Rev.* **2012**, *41*, 7333–7334.
[5] A. Proust, B. Matt, R. Villanneau, G. Guillemot, P. Gouzerh, G. Izzet, *Chem. Soc. Rev.* **2012**, *41*, 7605–7622.
[6] A. V. Anyushin, A. Kondinski, T. N. Parac-Vogt, *Chem. Soc. Rev.* **2020**, *49*, 382–432.
[7] A. Blazevic, A. Rompel, *Coord. Chem. Rev.* **2016**, *307*, *Part*, 42–64.
[8] A. J. Kibler, G. N. Newton, *Polyhedron* **2018**, *154*, 1–20.
[9] G. Izzet, B. Abécassis, D. Brouri, M. Piot, B. Matt, S. A. Serapian, C. Bo, A. Proust, *J. Am. Chem. Soc.* **2016**, *138*, 5093–5099.
[10] C. P. Pradeep, D. L. Long, G. N. Newton, Y. F. Song, L. Cronin, *Angew. Chem. Int. Ed.* **2008**, *47*, 4388–4391; *Angew. Chem.* **2008**, *120*, 4460–4463.
[11] B. Matt, J. Fize, J. Moussa, H. Amouri, A. Pereira, V. Artero, G. Izzet, A. Proust, *Energy Environ. Sci.* **2013**, *6*, 1504–1508.

[12] S. Schönweiz, S. A. Rommel, J. Kübel, M. Micheel, B. Dietzek, S. Rau, C. Streb, *Chem. Eur. J.* **2016**, *22*, 12002–12005.
[13] F. A. Black, A. Jacquart, G. Toupalas, S. Alves, A. Proust, I. P. Clark, E. A. Gibson, G. Izzet, *Chem. Sci.* **2018**, *9*, 5578–5584.
[14] J. M. Cameron, S. Fujimoto, K. Kastner, R.-J. Wei, D. Robinson, V. Sans, G. N. Newton, H. H. Oshio, *Chem. Eur. J.* **2017**, *23*, 47–50.
[15] E. Hampson, J. M. Cameron, S. Amin, J. Kyo, J. A. Watts, H. Oshio, G. N. Newton, *Angew. Chem. Int. Ed.* **2019**, *58*, 18281–18285; *Angew. Chem.* **2019**, *131*, 18449–18453.
[16] M. Ortiz, A. M. Debela, M. Svobodova, S. Thorimbert, D. Lesage, R. B. Cole, B. Hasenknopf, C. K. O'Sullivan, *Chem. Eur. J.* **2017**, *23*, 10597–10603.
[17] C. Yvon, A. J. Surman, M. Hutin, J. Alex, B. O. Smith, D.-L. Long, L. Cronin, *Angew. Chem. Int. Ed.* **2014**, *53*, 3336–3341; *Angew. Chem.* **2014**, *126*, 3404–3409.
[18] Y.-F. Song, R. Tsunashima, *Chem. Soc. Rev.* **2012**, *41*, 7384.
[19] C. Streb, *Dalton Trans.* **2012**, *41*, 1651–1659.
[20] R. Neumann, *Inorg. Chem.* **2010**, *49*, 3594–3601.
[21] J. M. Clemente-Juan, E. Coronado, A. Gaita-Ariño, *Chem. Soc. Rev.* **2012**, *41*, 7464–7478.
[22] S. Vanhaecht, J. Jacobs, L. Van Meervelt, T. N. Parac-Vogt, *Dalton Trans.* **2015**, *44*, 19059–19062.
[23] S. K. Petrovskii, V. V. Khistiaeva, A. A. Sizova, V. V. Sizov, A. V. Paderina, I. O. Koshevoy, K. Y. Monakhov, E. V. Grachova, *Inorg. Chem.* **2020**, *59*, 16122–16126.
[24] S. Schönweiz, S. Knoll, M. Anjass, M. Braumüller, S. Rau, C. Streb, *Dalton Trans.* **2016**, *45*, 16121–16124.
[25] H. C. Kolb, M. G. Finn, K. B. Sharpless, *Angew. Chem. Int. Ed.* **2001**, *40*, 2004–2021; *Angew. Chem.* **2001**, *113*, 2056–2075.
[26] A. Macdonell, N. A. B. Johnson, A. J. Surman, L. Cronin, *J. Am. Chem. Soc.* **2015**, *137*, 5662–5665.
[27] F. Odobel, M. Séverac, Y. Pellegrin, E. Blart, C. Fosse, C. Cannizzo, C. R. Mayer, K. J. Elliott, A. Harriman, *Chem. Eur. J.* **2009**, *15*, 3130–3138.
[28] M. Boujtita, J. Boixel, E. Blart, C. R. Mayer, F. Odobel, *Polyhedron* **2008**, *27*, 688–692.
[29] S. Amthor, S. Knoll, M. Heiland, L. Zedler, C. Li, D. Nauroozi, W. Tobaschus, A. K. Mengele, M. Anjass, U. S. Schubert, et al., *Nat. Chem.* **2022**, *14*, 321–327.
[30] Y. Ji, L. Huang, J. Hu, C. Streb, Y. F. Song, *Energy Environ. Sci.* **2015**, *8*, 776–789.
[31] D. Ma, L. Liang, W. Chen, H. Liu, Y. F. Song, *Adv. Funct. Mater.* **2013**, *23*, 6100–6105.
[32] R. Lamare, R. Ruppert, C. Boudon, L. Ruhlmann, J. Weiss, *Chem. Eur. J.* **2021**, *27*, 16071–16081.
[33] O. Dumele, J. Chen, J. V. Passarelli, S. I. Stupp, *Adv. Mater.* **2020**, *32*, 1907247.
[34] T. Keijer, T. Bouwens, J. Hessels, J. N. H. Reek, *Chem. Sci.* **2021**, *12*, 50–70.
[35] A. H. Proppe, Y. C. Li, A. Aspuru-Guzik, C. P. Berlinguette, C. J. Chang, R. Cogdell, A. G. Doyle, J. Flick, N. M. Gabor, R. van Grondelle, et al., *Nat. Rev. Mater.* **2020**, *5*, 828–846.
[36] C. L. Foster, C. A. Kilner, M. Thornton-pett, M. A. Halcrow, *Acta Crystallogr.* **2000**, *C*, 319–320.
[37] J. M. Barta, S. Díez-González, *Molecules* **2013**, *18*, 8919–8928.
[38] K. Schofield, M. R. Grimmett, B. R. T. Keene, *Heteroaromatic Nitrogen Compounds: The Azoles*, Cambridge University Press, Cambridge, **2011**.
[39] H. Maeda, H. Takayama, M. Segi, *Photochem. Photobiol. Sci.* **2018**, *17*, 1118–1126.
[40] H. Y. Nam, J. Seo, *Biopolymers* **2016**, *106*, 82–88.
[41] K. Kastner, A. J. Kibler, E. Karjalainen, J. A. Fernandes, V. Sans, G. N. Newton, *J. Mater. Chem. A* **2017**, *5*, 11577–11581.
[42] D. E. Herbranson, M. D. Hawley, *J. Org. Chem.* **1990**, *55*, 4297–4303.
[43] A. Kamal, N. Shankaraiah, K. L. Reddy, V. Devaiah, *Tetrahedron Lett.* **2006**, *47*, 4253–4257.
[44] A. P. Davis, A. J. Fry, *J. Phys. Chem. A* **2010**, *114*, 12299–12304.
[45] A. J. Fry, J. Touster, *J. Org. Chem.* **1986**, *51*, 3905–3907.
[46] K. Ritter, C. Pehlken, D. Sorsche, S. Rau, *Dalton Trans.* **2015**, *44*, 8889–8905.
[47] M. G. M. G. G. Pfeffer, C. Pehlken, R. Staehle, D. Sorsche, C. Streb, S. Rau, *Dalton Trans.* **2014**, *43*, 13307–13315.
[48] B. Kirchhoff, S. Rau, C. Streb, *Eur. J. Inorg. Chem.* **2016**, *2016*, 1425–1429.
[49] S. Tschierlei, M. Presselt, C. Kuhnt, A. Yartsev, T. Pascher, V. Sundström, M. Karnahl, M. Schwalbe, B. Schäfer, S. Rau, et al., *Chem. Eur. J.* **2009**, *15*, 7678–7688.
[50] M. Karnahl, S. Tschierlei, C. Kuhnt, B. Dietzek, M. Schmitt, J. Popp, M. Schwalbe, S. Krieck, H. Görls, F. W. Heinemann, et al., *Dalton Trans.* **2010**, *39*, 2359–2370.
[51] L. Troian-Gautier, C. Moucheron, *Molecules* **2014**, *19*, 5028–5087.
[52] D. Brynn Hibbert, P. Thordarson, *Chem. Commun.* **2016**, *52*, 12792–12805.
[53] P. Thordarson, *Chem. Soc. Rev.* **2011**, *40*, 1305–1323.
[54] L. Troian-Gautier, C. Moucheron, *Molecules* **2014**, *19*, 5028–5087

Manuscript received: November 8, 2022
Accepted manuscript online: December 15, 2022
Version of record online: February 9, 2023